Sandeep Jella[1]
Siemens Energy Canada Limited,
Montreal, QC H9P 1A5, Canada
e-mail: sandeep.jella@siemens-energy.com

Gilles Bourque
Siemens Energy Canada Limited,
Montreal, QC H9P 1A5, Canada

Pierre Gauthier
Siemens Energy Canada Limited,
Montreal, QC H9P 1A5, Canada

Philippe Versailles
Siemens Energy Canada Limited,
Montreal, QC H9P 1A5, Canada

Jeffrey Bergthorson
Department of Mechanical Engineering,
McGill University,
Montreal, QC H3A 0G4, Canada

Ji-Woong Park
Department of Mechanical Engineering,
University of Connecticut,
Storrs, CT 06269

Tianfeng Lu
Department of Mechanical Engineering,
University of Connecticut,
Storrs, CT 06269

Snehashish Panigrahy
Department of Chemistry,
National University of Ireland,
Galway H91 TK33, Ireland

Henry Curran
Department of Chemistry,
National University of Ireland,
Galway H91 TK33, Ireland

Analysis of Auto-Ignition Chemistry in Aeroderivative Premixers at Engine Conditions

The minimization of auto-ignition risk is critical to the design of premixers of high power aeroderivative gas turbines as an increased use of highly reactive future fuels (for example, hydrogen or higher hydrocarbons) is anticipated. Safety factors based on ignition delays of homogeneous mixtures are generally used to guide the choice of a residence time for a given premixer. However, auto-ignition chemistry under aeroderivative conditions is fast (0.5–2 ms) and can be initiated within typical premixer residence times. The analysis of what takes place in this short period necessarily involves the study of low-temperature auto-ignition precursor chemistry, but precursors can change with fuel and local reactivity. Chemical explosive modes (CEMs) are a natural alternative to study this as they can provide a measure for auto-ignition risk by considering the whole thermochemical state in the framework of an eigenvalue problem. When transport effects are included by coupling the evolution of the chemical explosive modes to turbulence, it is possible to obtain a measure of spatial auto-ignition risk where both chemical (e.g., ignition delay) and aerodynamic (e.g., local residence time) influences are unified. In this article, we describe a method that couples large eddy simulation (LES) to newly developed, reduced auto-ignition chemical kinetics to study auto-ignition precursors in an example premixer representative of real life geometric complexity. A blend of pure methane and di-methyl ether (DME), a common fuel used for experimental auto-ignition studies, was transported using the reduced mechanism (38 species/238 reactions) under engine conditions at increasing levels of DME concentrations until exothermic auto-ignition kernels were formed. The resolution of species profiles was ensured by using a thickened flame model where dynamic thickening was carried out with a flame sensor modified to work with multistage heat release. This paper is outlined as follows: First, a reduced mechanism is constructed and validated for modeling methane as well as DME auto-ignition. Second, sensitivity analysis is used to show the need for chemical explosive modes. Third, the thickened flame model modifications are described and then applied to an example premixer at 25 bar/890 K preheat. The chemical explosive mode analysis closely follows the large thermochemical changes in the premixer as a function of DME concentrations and identifies where the premixer is sensitive and flame anchoring is likely to occur. [DOI: 10.1115/1.4051460]

Introduction

In typical aeroderivative systems, fuel–air mixture reactivity is enhanced due to high compression ratios (20–40:1) and corresponding preheat (600—900 K). This results in a relatively smaller margin to auto-igniting. Accordingly, premixers are designed to achieve a residence time low enough to prevent auto-ignition, but high enough to obtain adequate mixing quality. Still other considerations such as the relationship between acoustics and fuel injection-to-flame time-lag also influence the premixer-residence time tradeoff. Premixers are designed to obtain residence time distributions that are at least 1–2 orders of magnitude below typical ignition delays. However, under engine conditions, precursor chemistry (intermediate radical formation without heat release) initiates even at these short time-scales. If this is allowed to progress to a critical point determined by local mixture concentrations, residence time, temperature, turbulent mixing rates, and ignition kernels with localized heat release can form and rapidly lead to a propagating flame in the premixer [1,2]. Therefore, to obtain insight into precursor formation, it is necessary to couple chemistry mechanisms that can accurately model low-temperature precursor (typically HO_2, H_2O_2, CH_2O) reaction pathways at high pressures to a stochastic description of the turbulent mixing process in the actual geometry [3,4].

Using two-dimensional direct numerical simulations, Mastorakos et al. [1] proposed that that auto-ignition is most likely to occur at a preferred mixture fraction at sites where scalar dissipation rates (SDRs) (micromixing rate of fuel) is low. Following this work, in a series of confined jet experiments, Markides and Mastorakos [5,6] found that kernels develop into localized "flamelets." These could extinguish under less reactive conditions but otherwise form secondary kernels which lead to a developing flame-front. Schmalhofer et al. [7] employed high speed chemiluminescence to investigate pressurized jets in a reheat context and described "initial" and "stabilizing" phases during which auto-ignition kernels form and coalesce. While initial kernels were expelled from the mixing section under less reactive conditions, the stabilizing phase is marked by an increased frequency of auto-ignition kernels eventually leading to an auto-ignition-assisted flame front. This "two-phase" description of the processes running

[1]Corresponding author.

Manuscript received December 3, 2020; final manuscript received May 30, 2021; published online October 13, 2021. Editor: Jerzy T. Sawicki.

up to heat release magnitudes at which point a flashback occurs invites a fundamental examination of the early precursors which form prior to any heat release.

Tracking fuel combustion chemistry "on-the-fly" (as opposed to tabulating it, for example) in large eddy simulation (LES) is a computationally expensive prospect [8,9] and requires careful treatment to ensure accurate computations of trace species. When higher hydrocarbon (C2+) fuel is present, the number of species required for an accurate description of intermediate chemistry greatly increases. Smaller mechanisms also invariably require accepting some assumptions such as quasi-steady-state [9], which may not always hold in low-temperature chemistry. A review of existing literature indicates that high fidelity simulations of auto-ignition are mainly restricted to direct numerical simulations and LES in simplified setups. These, nevertheless, yield important data on auto-ignition processes and help validate sophisticated numerical models with reasonable expense. Jones and Navarro-Martinez [10] applied LES with the *stochastic field* model for sub-grid closure and were able to model the random spots and flash-back as observed in the heptane experiments of Markides and Mastorakos [5]. Stankovic et al. [11] used the *conditional moment closure* model with LES to model the hydrogen jet experiments. Both works were able to qualitatively reproduce the two-phases (random spots, flashback) as observed in the experiment and emphasized the importance of the chemical mechanism.

The question of numerical resolution of the flame front was not discussed and it can be expected that this would be important under real gas turbine conditions. The need for flame thickening in the context of the stochastic field model was recently recognized by Picciani et al. [12]. Subgrid model sophistication, notwithstanding, Shulz et al. [13] used the *dynamically thickened flame* model to analyze auto-ignition of a rich premixed ethylene–air jet in hot crossflow. Though a model is not present for subgrid scale mixing (i.e., variance of the mixture fraction), the influence on predictions appears to have been small. An adjustment was needed to ensure flame thickening and was not triggered in the auto-ignition region.

Few works focus on precursor chemistry under high pressure/low temperature, turbulent conditions, which are characteristics of aeroderivative mixers. From the studies described above, it can be expected that the formation of random spots (or kernels) and kernel-induced flashback will continue to occur, perhaps more strongly under such conditions. To check a given premixer's robustness to auto-ignition, high pressure tests using spark-ignition or highly reactive fuels such as di-methyl ether (DME) blended with natural gas are carried out. Such tests, however, mainly assess adverse flame holding and do not (usually) allow optical access for deeper insight. To the best of our knowledge, no numerical studies on this topic have been reported using LES of real hardware under engine conditions. For this reason, this work focuses on precursor formation trends in a case study of a real, development, premixer with multiple fuel and air injections under high pressure conditions using DME as the fuel.

Chemical Mechanism for CH_4–Di-Methyl Ether Blends

Under high pressure engine conditions, low-temperature chemical pathways and pressure dependent reactions strongly influence ignition delay so that attempts to model ignition precursors should include these effects. A comprehensive chemical kinetic mechanism consisting of 171 species and 1221 reactions that includes these was developed in a hierarchical manner. The foundation of this detailed model is developed by a critical assessment of recent high-level calculations and experimental advances in rate constants and thermochemical properties. This newly updated base model contains the H_2/O_2 submechanism along with the C1–C3 reaction system to depict the pyrolysis and oxidation process of various hydrocarbon and oxygenated fuels: syngas, methane, methanol, ethane, ethylene, ethanol, propane, propene, and dimethyl ether. The low-temperature and high-temperature reactions for a DME submechanism are obtained from the recent work done by Burke et al. [14] where special attention was dedicated toward improving the model agreement against fundamental experiments over a wide range of pressure, temperature, and input operating conditions.

Directed relation graph aided sensitivity analysis (DRGASA) [15,16] techniques were employed to construct a 38 species/238 reactions reduced mechanism valid for the specified targets (ignition from 600–1600 K preheat, flame speeds for mixture equivalence ratios 0.3–2.0 and pressures from 7 to 41 atm) for mixtures ranging from pure CH_4 to pure DME. Figure 1 demonstrates a very good alignment between the detailed mechanism (lines) and the reduced one (symbols) with respect to auto-ignition delay and flame speeds for a range of pressures and stoichiometry for pure CH_4 and a DME blend of 15%. Higher preheat conditions for the flame speed validation are certainly possible but this entails a reduction of DME in the fuel blend as otherwise the blend increasingly exhibits auto-ignition-assisted flame propagation which results in an irrelevant laminar flame speed.

Kazakov et al. [17] emphasizes that causal pathways should be preserved during the mechanism reduction process: while ignition delays and flame speeds could remain less affected by the reduction process, precursor evolution could be significantly impacted with the result that detailed and reduced mechanism alignment but for different underlying physical reasons. Fewer reaction pathways are inherent to reduction strategies, but DRG targets were chosen carefully so that the precursors of interest were not affected. Figure 1 zooms in on selected precursor evolution and magnitudes in time (auto-ignition) and space (flame propagation). Good agreement shows that the reaction pathway reduction (at least in this case) has not affected these.

Finally, a small sample of comparisons of the reduced mechanism with experimental data is also shown in Fig. 2. Here, particle image velocimetry in high pressure stagnation flames was used to obtain axial velocity (u_p) profiles as described in Ref. [18]. The point of comparison for laminar flame speed is the location outlined by a circle in Fig. 2.

In each picture, flow is from right (unburned mixture) to left and $z = 0$ is the stagnation surface. The flame is seen as a relatively sudden increase in u_p. Discrepancies between the experiment (symbols) and model prediction (lines) are attributed to two-dimensional-effects in the burner not captured by the quasi-one-dimensional hydrodynamic model as used in Cantera. Agreement is excellent for both lean and rich flames. Given the foregoing validation, the reduced model was judged suitable for all computational fluid dynamics calculations detailed in the Case Study: Gas Turbine Premixer section.

As expected, the effect of DME in the fuel blend (in the example in Fig. 1, 15% by volume) strongly decreases the auto-ignition delay relative to pure CH_4, to time-scales comparable to the premixer's average residence time (1–3 ms). Auto-ignition dynamics (defined here as sensitivity to reaction pathways) are clearly different between the two fuels, and sensitivity analysis is needed to identify precursors of influence. In the larger scheme of things, an auto-ignition propensity metric should seek to avoid a dependence on arbitrarily selected precursors as these can depend on fuel as well as local composition states evolving after the introduction of fuel and oxidizer. This point will be made clearer in the following example.

To identify relevant precursors to auto-ignition of both CH_4 and DME blends, a "brute-force" ignition sensitivity analysis was carried out for typical engine conditions (40 bar, 850 K preheat, equivalence ratio 0.5) at early (1.5 ms) and near ignition (200.3 ms for CH_4 and 5.9 ms for DME) times. The 1.5 ms time was chosen to represent a typical premixer residence time when fuel and air have mixed and thermal stratification due to hot air and cold fuel is reduced. The ignition sensitivity, S_τ, is defined with respect to the rate constant, k, for i reaction pathways. Following Ji et al. [19], this is defined as $S_\tau = \partial\tau\partial k_i$ and is normalized by $k_i\tau$. Although a wide range of pressures and operating conditions were considered, baseload-relevant results are summarized in a

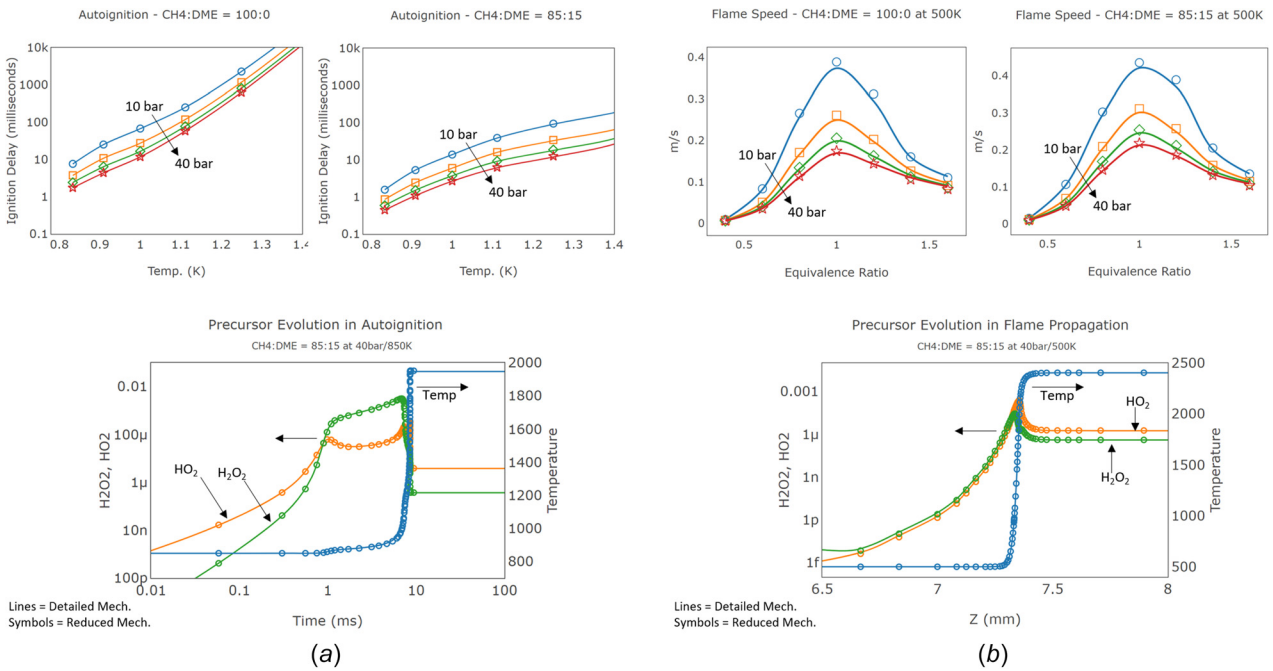

Fig. 1 Validation of reduced mechanism and sensitivity analysis for pure CH_4 and 15% DME blend: picture column (*a*) auto-ignition and (*b*) flame speed and corresponding precursor evolution

normalized sensitivity plot (simply termed as "Sensitivity") in Fig. 3. Positive values on the x axis imply that reactions *pace* auto-ignition while negative values *accelerate* it. The top ten reactions are ordered in decreasing order of influence to auto-ignition. An inspection shows that species and pathways both change with respect to influencing the auto-ignition delay depending on where they are on the trajectory. For pure CH_4 (Fig. 3(*a*)), at a relatively early time (1.5 ms), which represents flow about half-way through a typical premixer, the auto-ignition delay is rate-controlled by methyl (CH_3) radical formation due to methane oxidation (i.e., $CH_4 + O_2 \rightarrow CH_3 + HO_2$). After CH_3 is produced, it accelerates auto-ignition through its own oxidation. At this relatively early time, few other pathways have as much influence. Much later, however, at the point of ignition (Fig. 3(*b*)), it can be seen that ignition is sensitive to the availability of hydrogen peroxide (H_2O_2) and the methylperoxy radical (CH_3O_2) and the hydroperoxyl radical (HO_2) and formaldehyde (CH_2O). The appearance of HO_2 is clearly very important in accelerating the production of H_2O_2 from several sources (CH_4, CH_2O, CH_3O) as almost all molecules it reacts with have a positive correlation with auto-ignition.

Aside from this example, prior studies of fully ignited flames (for example, Ref. [20] and [21]) have identified the hydroperoxyl radical (HO_2), hydrogen peroxide (H_2O_2), and formaldehyde (CH_2O) molecules to be precursor species, capable of accelerating the formation of auto-ignition kernels associated with heat-

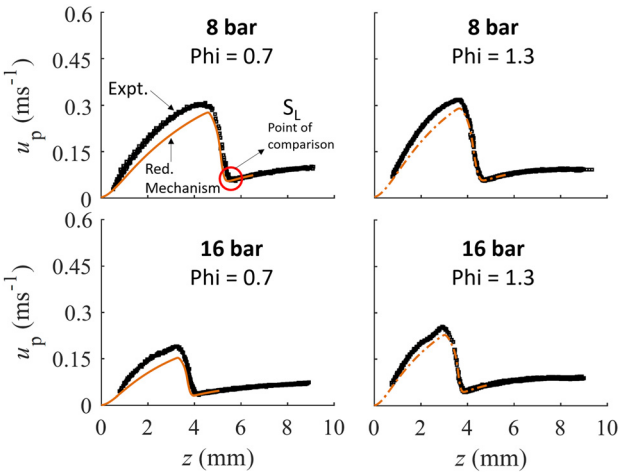

Fig. 2 Comparison between experiment and reduced model

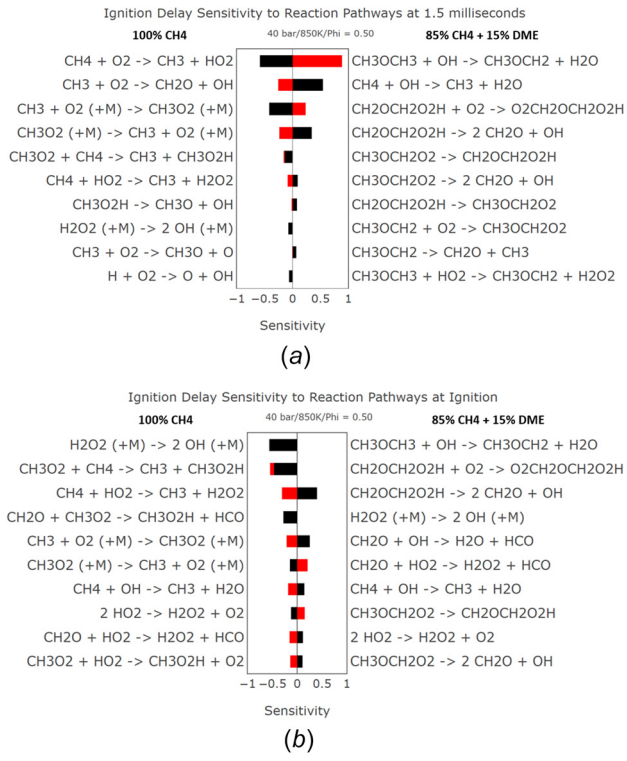

Fig. 3 Pathway importance at (*a*) pre-ignition (1.5 ms) and (*b*) ignition stages. Red bars: CH_4 (100%), black bars: CH_4–DME blend (85%:15%).

release. With DME, the 1.5 ms time instant is much closer to the ignition delay time. Accordingly, it is seen that DME's (as well as some intermediates') reaction with OH remains of primary influence at both pre-ignition (no heat release) and ignition (thermal runaway) times. Low temperature chain branching reactions involving $CH_3OCH_2O_2$ and $CH_2OCH_2O_2H$ are rate-controlling but produce OH and CH_2O, which subsequently accelerate the combustion process. Though OH is of importance to auto-ignition in the DME blend here, the reactions between precursors already identified from the pure CH_4 analysis, i.e., between HO_2, H_2O_2, and CH_2O, continue to remain important.

The wide range of precursor influences makes it difficult to simply interpret raw precursor magnitudes as a measure of auto-ignition sensitivity as in real systems this can change in time and space. For more reactive fuels, the near instant appearance of intermediate radicals make it difficult to choose any of them to assess the auto-ignition risk for different premixer geometries. This is expected to only become more complex with an increase in the carbon number of the fuel as heavier radicals are primary precursors during fuel pyrolysis. Therefore, it is proposed that precursor fields can be interpreted more usefully via an explosive mode analysis which assesses the entire thermochemical state as a system.

Chemical Explosive Mode Analysis

With its original presentation in the computational singular perturbation [22,23] framework, the linear stability analysis of a combustion process can be used to assess system dynamics. The general thermochemical change of the state vector, $\mathbf{\Phi} = [Y_k, T]$, comprising of k species mass fractions Y and temperature T, is due to reaction $\boldsymbol{\omega}$ and transport (mixing) $\mathbf{s}$

$$\frac{D\mathbf{\Phi}}{Dt} = \boldsymbol{\omega}(\mathbf{\Phi}) + \mathbf{s}(\mathbf{\Phi}) \tag{1}$$

If an infinitesimal perturbation is applied to the chemical term, $\boldsymbol{\omega}$, the difference between the perturbed and original states may be written as $\epsilon_\Phi = \mathbf{\Phi}' - \mathbf{\Phi}$, where $\mathbf{\Phi}'$ is the perturbed temperature or mass fraction. The subsequent evolution of ϵ_Φ is estimated using a Taylor series [24] to expand the derivative applied to the reaction term in Eq. (1). This is approximated to the leading order

$$\frac{d\epsilon_{\mathbf{\Phi}}}{dt} \approx \frac{\partial \boldsymbol{\omega}(\mathbf{\Phi})}{\partial \Phi}(\mathbf{\Phi}' - \mathbf{\Phi}) = \mathbf{J}_{\mathbf{\Phi}} \cdot \epsilon_{\mathbf{\Phi}}(t) \tag{2}$$

where $\mathbf{J}_{\mathbf{\Phi}}$ is the chemical Jacobian matrix. The likelihood of the perturbation to cause the chemical state to return or deviate from its trajectory may be assessed by extracting the eigenvalues of $\mathbf{J}_{\mathbf{\Phi}}$. The diagonalization of $\mathbf{J}_{\mathbf{\Phi}}$ yields the explosive eigenmodes, $\mathbf{\Lambda}$, each of which is associated with the thermochemical state (left and right eigenvectors, $\mathbf{\Phi}_L$ and $\mathbf{\Phi}_R$, respectively) so that $\mathbf{J}_{\mathbf{\Phi}} = \mathbf{\Phi}_L \cdot \mathbf{\Lambda} \cdot \mathbf{\Phi}_R$. If the real parts of $\mathbf{\Lambda}$ are sorted in descending order, the largest eigenvalue is termed as the "most explosive" mode [25], λ_{exp}. If λ_{exp} is positive, then the perturbation grows exponentially whereas a negative value pushes the thermochemical state toward equilibrium. λ_{exp} can span several orders of magnitude, and Lu et al. [25] casts the eigenmodes more conveniently in logarithmic equivalents, $\text{LE} \equiv \text{sign}(\lambda_{\text{exp}}) \log_{10}(1 + |\lambda_{\text{exp}}|)$. While chemical explosive modes (CEMs) have been widely used to study flames [25–27], they are generally applicable to any scenario where chemical kinetics primarily govern the evolution of the chemical state to ignition.

This is illustrated in Fig. 4 where an auto-ignition profile of temperature is analyzed for two different fuels: pure CH_4 which has only a single stage of ignition and a DME blend where ignition happens in two stages. Stage 1 ignition in this case is a (relatively) mild heat release of ~100 K during the low-temperature chemistry phase, while stage 2 is the thermal runaway leading to full ignition. The zero-crossing on the horizontal axis may be interpreted as the auto-ignition delay for each stage. The advantage of using CEMs can be seen—they can clearly highlight the nonlinearities of the auto-ignition delay curve and provide valuable pre-ignition information.

The temperature profiles in Fig. 4 are colored by the local characteristic explosive time-scale $(1/\lambda_{\text{exp}})$ and are overlaid with LE (black line). The sudden growth of LE marks the movement of the system to auto-ignition after which LE suddenly drops to a negative value in the postflame zone. This is around 200 ms for CH_4, while it is just ~2 ms for the selected DME blend. Despite the long ignition delay for CH_4, the CEM evolution shows that there is a characteristic "dip" around 2 ms which plateaus until ignition. This is the region of low-temperature chemistry without heat release. The time-scale is such that this effect will be present at premixer residence time scales and can be used in combination with the early stages of precursor development.

In premixer flows, system perturbations arrive in the form of turbulent mixing which affects the thermochemical state as well as induces a wide range of local residence times. In this context, the time scale of the explosive modes can be used in conjunction with a local mixing time-scale estimate to define an "explosive" Damköhler number distribution as proposed by Lu et al. [25] in the analysis of fully ignited flames. Therefore, the evolution of CEMs in LES can provide the necessary coupling between the zero-dimensional reactor analysis and the complexity of combustion chemistry in turbulent flows.

Case Study: Gas Turbine Premixer

To demonstrate the precursor formation and analysis, an experimental premixer was chosen. A section of the geometry is shown in Fig. 5. The premixer features multiple jets injecting pure air into a cross stream of gaseous fuel. The distributed injection of air and fuel results in a range of residence times that has been found to significantly damp intermediate frequency dynamics for a wide range of operating conditions. The theoretical basis and operational performance of the premixer have already been described in detail by Scarinci et al. [28]. While the in-service product was engineered to have a delay over six times shorter than the worst case auto-ignition delay for natural gas [28], a known nonoptimal developmental concept was chosen for this study for illustration purposes.

Three cases were run at 25 bar with an air temperature of 890 K, a fuel temperature of 323 K, and a nominal mixture equivalence ration of 0.56. These represent typical part-load conditions. Pure CH_4 was blended with an increasing amount of DME until natural auto-ignition took place. Cases corresponding to 18%, 30%, and 40% DME will be studied.

Numerical Setup. ANSYS FLUENT v19.3 was used for all the LES calculations. To model subgrid stresses, the transported kinetic energy model of Kim and Menon [29] was used. Since it was necessary to consider the possibility of a flame front developing in a confined space, partially reflective boundary conditions were used to allow pressure waves to exit the computational domain and allow natural fluctuations of air and fuel flow rates. A bounded central differencing scheme was used for the convective terms in the momentum equation, while the diffusion terms were discretized using pure central differencing. Second order upwinding was used for all scalars. The temporal terms were discretized using a second order backward differencing scheme. Although the stability of the numerics allows Courant-Friedrichs-Lewy numbers larger than 1, a time-step restricting the Courant-Friedrichs-Lewy number to less than 0.5 was chosen. The mesh cell size in the premixer was 0.2 mm or lesser. PyJac [30] was used to generate analytical expressions for the Jacobian analysis.

Dynamically Thickened Flame Model. The dynamically thickened flame model (DTFM) was chosen because auto-ignition may lead to a propagating flame in the premixer with a thickness

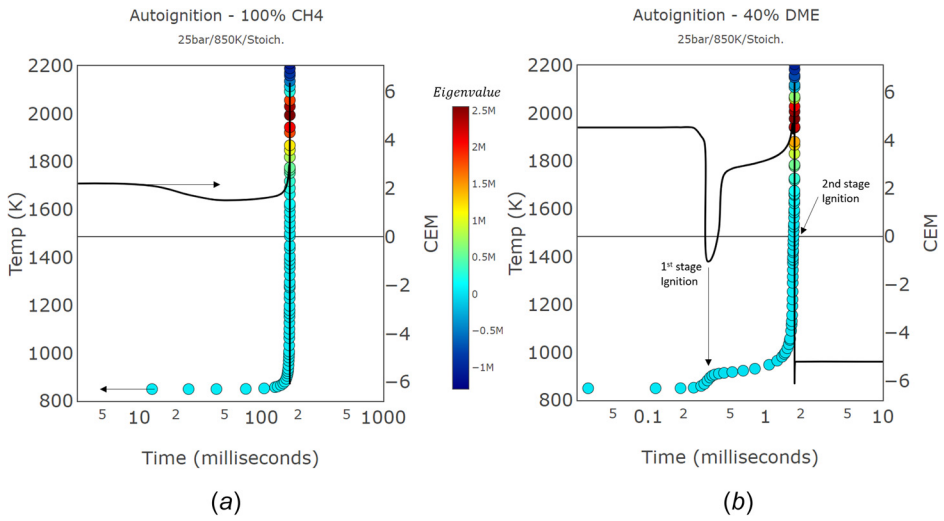

Fig. 4 The evolution of most explosive modes during auto-ignition for (*a*) pure CH_4 and (*b*) DME blend

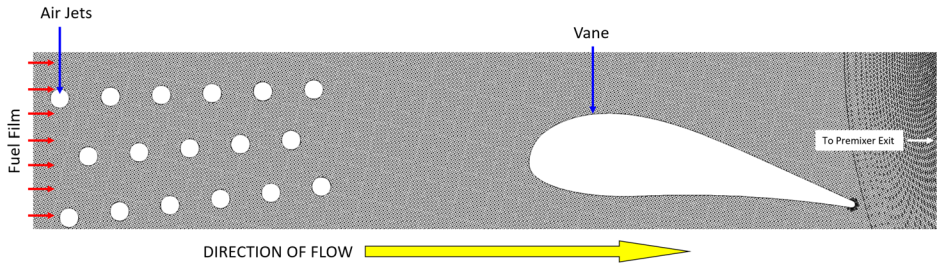

Fig. 5 Example premixer and mesh

that cannot be resolved by the mesh. The DTFM thickens the flame in a controlled manner [31] to propagate at the same laminar flame speed as the nonthickened one on a given mesh. While full descriptions of the model may be obtained in other works (e.g., Refs. [31] and [32]), it is sufficient to recall that the laminar flame speed, $S_L \propto \sqrt{D\omega}$, so that the transformation for the chemical source $\omega \rightarrow \omega/F$ and diffusivity $D \rightarrow FD$ leaves S_L unchanged. $F = 1 + (N\Delta/\delta_f - 1)S$, where F is the local thickening factor applied after determining the number of points, N, that a flame of thickness δ_f is thickened over for a given filter size Δ. Here, attention is focused on an issue with the usual definition of the flame sensor, S. To ensure thickening is restricted to a small spatial envelope of the flame front, the dynamic flame sensor S was used to track the flame front and trigger thickening is based on a fuel reaction or heat release rate, ω

$$S \equiv \mathrm{MAX}\left[\tanh\left(\beta\frac{\omega}{\omega_{\max}}\right), 0\right] \tag{3}$$

where β is used to control sensor sensitivity. Higher values cause the sensor to activate at smaller values of ω. β and was set to 50 in this work. $\omega_{\max}$ is usually obtained from a precursor laminar flame simulations. For very small values of ω, the sensor is essentially zero and flame thickening is not triggered here as $S = 0$. A difficulty arises with this definition, as higher hydrocarbons such as DME exhibit multiple ignition stages during auto-ignition.

Figure 6 shows that S is triggered in the first stage/low-temperature ignition zone at approximately 0.2 ms simply because of nonzero fuel consumption (net destruction rate of DME overlaid as a red line). In addition, $\omega_{\max}$ from a laminar flame speed calculation is irrelevant and a flame thickness has no relevance in this region. If the thickening is triggered, the reaction source is lowered by a factor F, which will artificially increase the auto-ignition delay. When low temperature ignition stages are possible, additional criteria are needed to ensure that thickening is constrained only to the highly exothermic flamelet kernels. Given that auto-ignition leading to a flame propagation occurs under stratified mixture conditions, a predominantly premixed mode of burning is expected.

This implies that S as defined above is not valid for the first stage auto-ignition regime and should be constrained to only work with "sharp" flame fronts that are not solved by the base computational fluid dynamics grid. In this study, the "standard" definition of the sensor, S, is extended as follows:

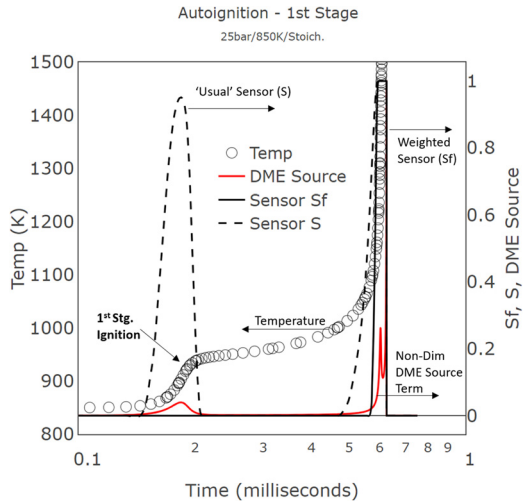

Fig. 6 OH weighted flame sensor

(1) The resolved mixture fraction SDR defined as $N_z \equiv D\,\nabla Z \cdot \nabla Z$ is calculated. The values of N_z smaller than 0.1 indicate that mixing is practically complete. Using this, the DTF model is only switched on in regions where reactants are formally premixed.
(2) The concentration of OH can be used to isolate the low temperature regime from the high temperature ignition. The flame sensor can be redefined as

$$S_f \equiv \mathrm{MAX}\left[\tanh\left(\beta \frac{\omega}{\omega_{\max}} \cdot \left(\frac{Y_O H}{Y_O H|_{\max}}\right)^a\right), 0\right] \tag{4}$$

where the exponent a can be tuned to lower the sensitivity of the sensor's propensity to pick up first stage ignition. In this study, the best choice was found to be $a = 0.5 - 0.8$. Equation (4) ensures thickening is not prematurely triggered as shown in comparison to S in Fig. 6. Between 0.5 ms and 0.7 ms on the horizontal axis (sharp temperature rise), the behavior of the OH-weighted sensor (i.e., S_f, solid line) is similar to the conventional sensor (S, dashed line) but also has the advantage of a more compact envelope, which nevertheless covers the two peaks of the chemical source term for DME.

The DTF model was validated by comparing a uniform, coarse, 40-cell Fluent mesh with 10 cells across the flame front with a reference, highly resolved one-dimensional Cantera simulation of a laminar flame. Figure 7 shows the correspondence both in thickened space (for the temperature) and in unthickened space (profiles from thickened space are transformed back using the scaling relationship as described in Ref. [33]). The profiles are shifted on the horizontal axis for clarity.

The foregoing treatment, therefore, ensures that mesh resolution issues do not impact kernels with well-defined, sharp flame fronts. Figure 7 shows that even stiff species such as formyl radical may be adequately resolved. Note, however, that this model only applies in the event of the formation of a well-defined flame-front. In the absence of the flame (i.e., spatially broad kernels), there is no turbulence-chemistry interaction at the subgrid scale and each cell is treated as a simple constant pressure reactor with transport effects coming from the velocity field (resolved and subgrid). This is a point worth investigating in a future work, but here we rely on a fine mesh to minimize the error due to the lack of a subgrid mixing model.

Large Eddy Simulation-Dynamically Thickened Flame Model: Results and Discussion. All simulations exhibit typical turbulence effects as illustrated for the 40% DME case in Fig. 8. Figure 8 (left) shows that at 40% DME, second-stage/thermal runaway ignition has been achieved at the trailing edge of the guide vane, characterized by the highly exothermic OH radical. In the guide vane region (leading to trailing edge), the SDR field is nearly nonexistent (Fig. 8, center) as high levels of vorticity (nearly 100,000–200,000/s) rapidly dissipate fuel gradients which are first formed in the upstream air jet section. Accordingly, the preferred mixture fraction for auto-ignition as described by Mastorakos et al. [1] in the vane section is whatever the premixed state is at this location. If auto-ignition occurred here (say due to excess residence time), a rapid transition to a premixed flame with flashback behavior is expected. Far upstream, however, the SDR is high near the point of fuel injection and this certainly influences the net reaction rate of auto-ignition chemistry as described in Ref. [1]. Figure 8 also shows that strongly turbulent structures persist throughout the domain. It can be expected that this will result in very thin (order of 0.1 mm) flames with flamelet-like characteristics propagating via a flame surface increase in addition to being auto-ignition assisted [26].

Results are now compared for three different levels of DME in Fig. 9 which shows nondimensionalized temperature contours in the left column and corresponding CEM logarithmic equivalents (LE) in the right. The temperatures were nondimensionalized by the air preheat. Values larger than 1 indicate excess temperature from exothermic processes. Values less than 1 are due to hot air mixing with cold fuel. As the turbulence "perturbs" the mixing state, the instantaneous propensity to auto-ignite also changes.

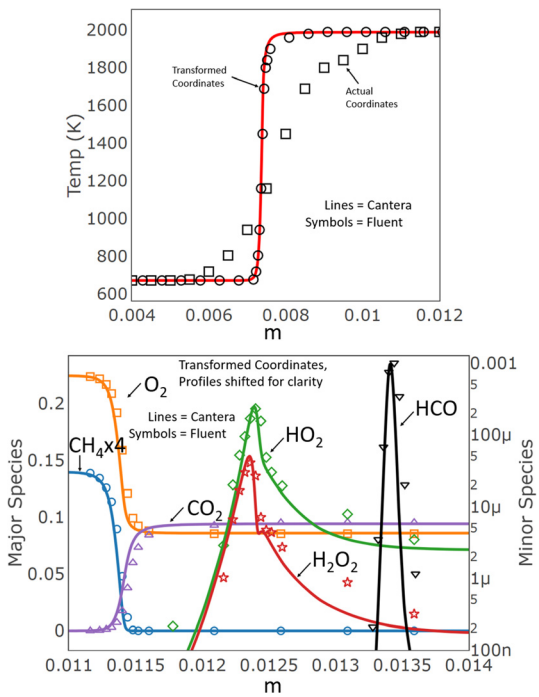

Fig. 7 DTF model: temperatures and species

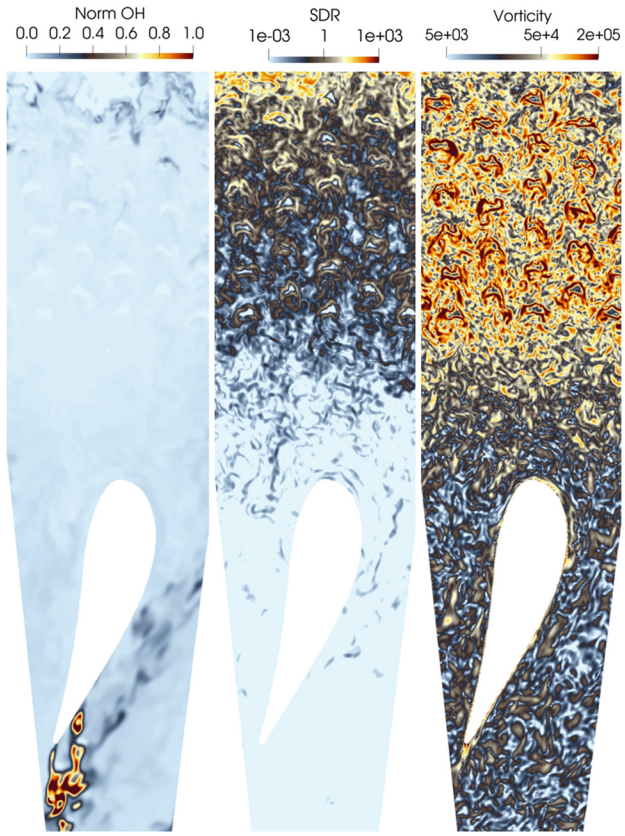

Fig. 8 OH radical, SDR of fuel and vorticity—40% DME

The CEM fields are useful since they indicate where the premixer is most susceptible to auto-ignition. For the lower DME cases, the pictures in Fig. 9 are representative of a statistically periodic state and no further heat release was noted. However, at 40% DME, a selected instant before the onset of flashback is shown. This choice will be explained below.

At 18% DME, there is a small increase of temperature above that obtained from the mixture of hot air and cold fuel. This rise is consistent with the zero-dimensional calculations of Fig. 4 (right). While the temperature rise is difficult to visualize in the temperature contours, the CEMs clearly show a broad region of negative value (black space) in the air jet region seen in the right column of Fig. 9 (top picture). After this region, the CEMs become positive again. If residence time were to permit, the next stage of ignition will occur with a sharp temperature rise with CEMs correspondingly becoming negative for the second time (again as in Fig. 4). In the present case, the local premixer residence time does not permit this to happen and the CEMs continue to stay positive.

As the DME concentration is increased to 30%, the two stages of ignition move closer to each other so that the black, negative CEM regions in the 30% DME case have shrunk. With the increased reactivity, first stage ignition temperatures increase. The amplitude of the explosive modes also increase to approximately 1 order of magnitude above that of the 18% case. Exothermic kernels (outlined in black circles in the right column of Fig. 9, middle picture) begin to appear with the increasing frequency. This is consistent with the observations by Schmalhofer et al. [34] where kernels appear and coalesce, eventually filling the mixing duct. The increase in CEM (λ_{exp}) magnitudes implies faster chemical time scales, τ_c where $\tau_c = 1/\lambda_{\text{exp}}$. This does not imply a decreased ignition delay but it can be interpreted to mean that the system is relatively slower to recover from a perturbation that could potentially nudge it to auto-ignite.

At 40% DME, this sensitivity reaches a tipping point and a thermal runaway was observed in the premixer as the ignition delay is lower than the mean residence time. Accordingly, the zone of heat release expands beyond that shown in the corresponding pictures of Fig. 9 due to the onset of a flashback. An early instant is chosen to preserve continuity between the lower DME cases and the stages of auto-ignition prior to the flashback. As in the other cases, exothermic kernels continue to increase and ignite in the free-stream, collecting in the wake of the vane. The explosive modes show more clearly than the temperature field that the location of a second stage ignition (high heat release) appears to be forming in the guide vane region. With respect to the guide vane's trailing edge, the heat release at this instant is representative of second stage ignition, though a second negative CEM region (postflame region) is not evident at this instant. The all-positive eigenmodes, therefore, point to an increased sensitivity of this region and establish it as the primary component that is (statistically) most likely to meet all the criteria for a flame stabilization and would benefit from some re-engineering to mitigate flame anchoring. For this, a few considerations with respect to the flow-field and chemical time-scales are now discussed.

Timescale Analysis. Figure 10 shows contours of the nondimensionalized velocity profile. As observed by Schulz et al. [27], each of the air jets (shown as red "spots" in the upstream mixing section) is associated with a wake on the lee side, which could potentially anchor a flame. Flow decelerates between the last row of air jets and the guide vane leading edge after which it is strongly accelerated. The residence time may be inferred from this picture as accumulating in the low-velocity wake (dark-blue) regions and correlates quite well with the formation of the early precursors as characterized by positive CEM modes under all conditions as seen in Fig. 9. In particular, at 40% DME, though the vane trailing edge experiences high temperatures, several places in the upstream mixing section exhibit chemical explosive modes at comparable magnitudes. This implies that a propagating flame can travel far upstream of the vane. The combustion regime is likely to be very complicated as characteristics of both diffusion and premixed flames can apply. Since Fig. 8 indicates that turbulent structures are particularly strong in this region, it is of interest to compare characteristic flow and chemical time scales as obtained by the reciprocal of the eigenvalues, τ_c. For a flow time scale, the resolved strain tensor (S_{ij}) is chosen, based on the Smagorinsky model where $\tau_{\text{mix}} = \Delta/u'_\Delta = 1/C_s \cdot 1/\sqrt{2S_{ij}S_{ij}}$. Here, C_s is the Smagorinsky constant, and u'_Δ is the turbulent velocity at the subgrid (Δ) scale. This allows the definition of an explosive-mode based Damöhler number where $\text{Da}_{\text{exp}} = \tau_{\text{mix}}/\tau_c$.

Figure 11 corresponds to the chemical time scales obtained from the reciprocal of the chemical explosive modes ($1/\lambda_{\text{exp}}$). Though these are very intermittent and range several orders of magnitude as observed in Fig. 9, there is a significant correlation with temperature as it strongly contributes to the CEM (and by extension to the chemical timescale, τ_c). This is seen when conditional averages of τ_c are taken with respect to temperature in Fig. 11. Though each CEM curve in Fig. 11 represents a completely different state of turbulence-chemistry interaction, the chemical explosive modes unify local residence time, stoichiometry, and temperature effects into clear trends. The Da numbers

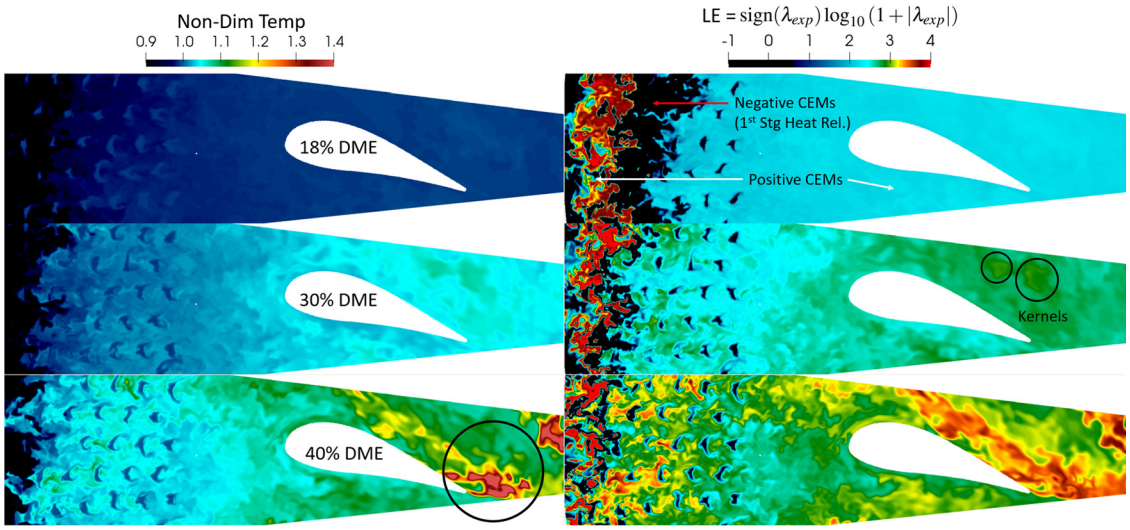

Fig. 9 (Left) Nondimensionalized temperature and (right) chemical explosive modes

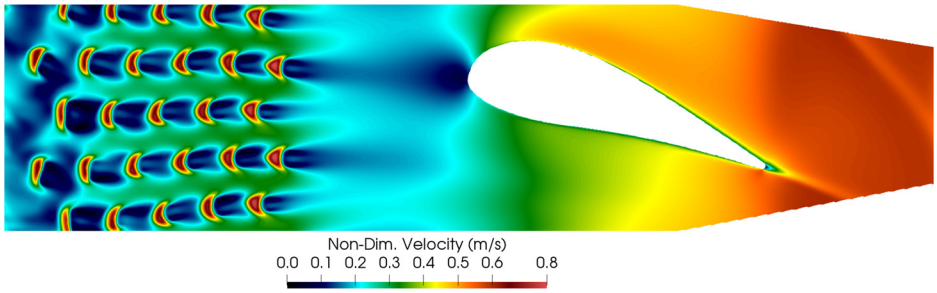

Fig. 10 Velocity profile

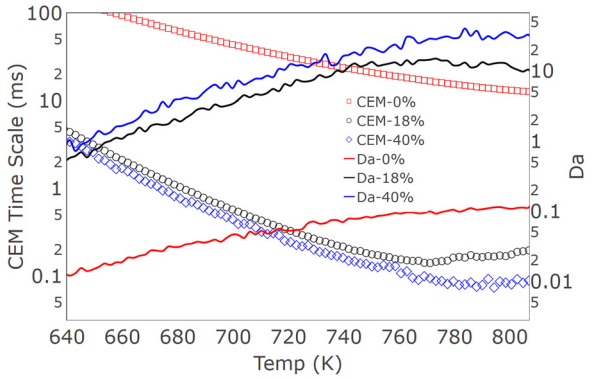

Fig. 11 Chemical timescales (symbols) and Damköhler numbers (lines) conditionally averaged on temperature

then translate these into an ability to infer the local combustion regime. In Fig. 11, a case with pure methane (shown as the 0% curves) is also included to highlight the influence of DME on the fuel–air mixture. Relative to this case, even a trace amount of DME can cause the chemical time scales drop by almost 2 orders of magnitude. This highlights the strong effects of fuel contamination by higher hydrocarbons even in small quantities. An interesting observation is that explosive mode time scales do not decrease with the further increase in DME (curves for 18%–40%) nearly overlap. This is unlike the ignition delay which continues to decrease with the increase in the DME content in the fuel.

Since it can be expected that the high turbulence levels will predominantly cause flames burning (stratified) premixed regime, the Da number can be used to infer the location of kernels in the combustion regime (e.g., as obtained in a Borghi diagram). The pure methane case indicates Da well below 1 while the DME cases range from 10 to 30. This situates flame kernels in very different combustion regimes depending on the Da: flame kernels formed in the methane case may be expected to be thicker and more prone to heat losses than those formed in the DME cases. Figure 12 shows spatial distributions of the conditionally averaged Damköhler numbers for pure methane and for the 40% DME case and highlights different components of the premixer with respect to local sensitivities (i.e., auto-ignition susceptibility). It is likely that auto-ignition risk in the pure methane case could be lowered by modifying the guide vane section (for example, accelerating the flow here) as the mixing section is relatively free of auto-ignition precursors due to the low Da. However, the DME case clearly shows that while the vane section will need to be modified, the air jet section will also need to ensure that precursors do not have time to build up. A full discussion of the improvements that could be made is out of the scope here but results highlight the main physics that should be taken into account when assessing (experimentally or numerically) premixers using highly reactive fuels.

In summary, the CEM-based chemical timescales are a useful upper bound to premixer residence time choices and complement the typical metrics used to assess auto-ignition risk. Access to spatial distributions of chemical reactivity and flow-turbulence interaction brings additional insight to optically inaccessible high pressure tests.

Conclusions

A method for modeling auto-ignition risk using DME in an example aeroderivative premixer has been described. The formation of auto-ignition kernels leading to an incipient flame was observed and is qualitatively consistent with observed

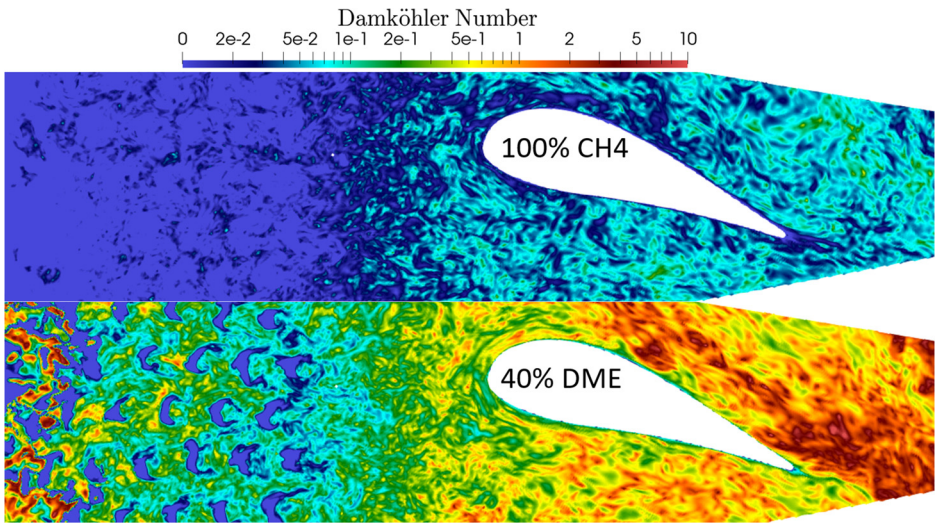

Fig. 12 Spatial distribution of Damköhler number

mechanisms in the literature. A new 38-species reduced mechanism capable of accurately modeling ignition delay as well as flame speed for a wide range of pressures was validated and then fully transported with a modified dynamically thickened flame model. Simulations were carried out for a range of DME concentrations in a manner similar to a typical rig test (ramping up) until natural auto-ignition occurred. In the example premixer used, the exothermic kernels develop and coalesce. Chemical explosive mode analysis was used to highlight regions of the premixer that could be susceptible to auto-ignition and demonstrated correlation to sites of high thermochemical sensitivity. It is, therefore, proposed as a convenient measure of auto-ignition risk when the thermochemical state is available as part of the calculation and a fine-grained analysis is required to bridge rig experiments and reduced order modeling. The strong influence of low temperature chemistry at high pressures was clearly shown and justifies the use of the newly developed reduced mechanism. The effects of subgrid scale mixing was reserved for a future work.

Acknowledgment

Computations were performed on the Niagara supercomputer at the SciNet HPC Consortium at the University of Toronto. Dr. Jim Rogerson of Siemens Industrial Turbomachinery Limited, Lincoln, UK, is thanked for his detailed review.

Nomenclature

Acronyms

C^{2+} = higher hydrocarbons
CEM = chemical explosive mode
DME = di-methyl ether
DRGASA = directed relation graph aided sensitivity analysis
DTFM = dynamically thickened flame model
LE = logarithmic equivalent of a CEM
LES = large eddy simulation

Symbols

C_s = Smagorinsky constant
$\mathrm{Da}_{\mathrm{exp}}$ = explosive Damköhler number
$\mathbf{J}_{\mathbf{\Phi}}$ = Jacobian matrix
N_z = scalar dissipation rate of mixture fraction
S_{ij} = strain tensor
u'_{Δ} = turbulent velocity
Y_{OH} = mass fraction of OH
$\mathbf{\Lambda}$ = eigenvalue matrix
λ_{exp} = most explosive eigenmode
τ_c = chemical timescale
$\mathbf{\Phi}$ = state vector of species mass fractions and temperature
$\mathbf{\Phi}_{L/R}$ = left/right eigenvectors
ω = CH_4 destruction rate

Appendix: Mechanism Reduction Process

In DRG, species couplings are first mapped to a graph, and species that are important to the selected starting species (e.g., H atom in this study) are identified through a recursive graph search. A threshold value of 0.3 is used to control the worst-case reduction error, resulting in an 85-species skeletal model. DRGASA is then applied with ignition delay and perfectly stirred reactor residence times as target parameters.

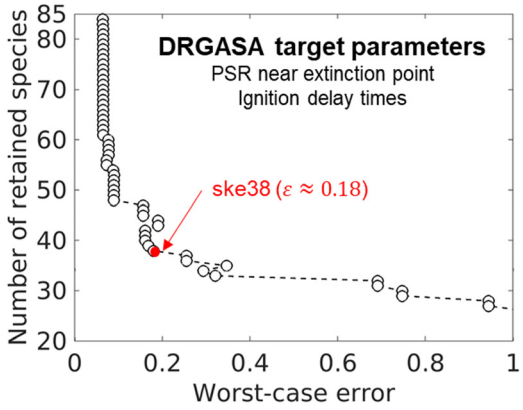

Fig. 13 Retained species versus error

Figure 13 shows the reduction curve in DRGASA with the number of retained species as a function of worst-case error in target parameters. It is seen that while the number of species is rapidly reduced below a worst-case error threshold of 0.2, a significant gap is observed near 0.2 with an additional removal of few species. Thus, a 38-species skeletal model is obtained by choosing an error-threshold of 0.18. Next, time-scale based reduction is performed using the same sampled reaction states used in the skeletal reduction as before, and 13-species are identified as global quasi-steady-state species using a method based on computational singular perturbation [35]. This yields, a 25-species reduced model for the CH_4/DME blend. In this study, however, the 38-species mechanism was used.

References

[1] Mastorakos, E., Baritaud, T., and Poinsot, T., 1997, "Numerical Simulations of Autoignition in Turbulent Mixing Flows," Combust. Flame, **109**(1–2), pp. 198–223.
[2] Markides, C., and Mastorakos, E., 2005, "An Experimental Study of Hydrogen Autoignition in a Turbulent Co-Flow of Heated Air," Proc. Combust. Inst., **30**(1), pp. 883–891.
[3] Mastorakos, E., 2009, "Ignition of Turbulent Non-Premixed Flames," Prog. Energy Combust. Sci., **35**(1), pp. 57–97.
[4] Goy, C., Moran, A., and Thomas, G., "Autoignition Characteristics of Gaseous Fuels at Representative Gas Turbine Conditions," ASME Paper No. 2001-GT-0051.
[5] Markides, C. N., and Mastorakos, E., 2008, "Flame Propagation Following the Autoignition of Axisymmetric Hydrogen, Acetylene, and Normal-Heptane Plumes in Turbulent Coflows of Hot Air," ASME J. Eng. Gas Turbines Power, **130**(1), p. 011502.
[6] Markides, C. N., and Mastorakos, E., 2011, "Experimental Investigation of the Effects of Turbulence and Mixing on Autoignition Chemistry," Flow, Turbul. Combust., **86**(3–4), pp. 585–608.
[7] Schmalhofer, C. A., Griebel, P., and Aigner, M., 2018, "The Influence of Carrier Air Preheating on Autoignition of Inline-Injected Hydrogen–Nitrogen Mixtures in Vitiated Air of High Temperature," ASME J. Eng. Gas Turbines Power, **140**(3), p. 031502.
[8] Lu, T., and Law, C. K., 2009, "Toward Accommodating Realistic Fuel Chemistry in Large-Scale Computations," Prog. Energy Combust. Sci., **35**(2), pp. 192–215.
[9] Felden, A., Pepiot, P., Esclapez, L., Riber, E., and Cuenot, B., 2019, "Including Analytically Reduced Chemistry (ARC) in CFD Applications," Acta Astronaut., **158**, pp. 444–459.
[10] Jones, W., and Navarro-Martinez, S., 2009, "Numerical Study of n-Heptane Auto-Ignition Using LES-PDF Methods," Flow, Turbul. Combust., **83**(3), pp. 407–423.
[11] Stanković, I., Triantafyllidis, A., Mastorakos, E., Lacor, C., and Merci, B., 2011, "Simulation of Hydrogen Auto-Ignition in a Turbulent Co-Flow of Heated Air With LES and CMC Approach," Flow, Turbul. Combust., **86**(3–4), pp. 689–710.
[12] Picciani, M., Richardson, E., and Navarro-Martinez, S., 2018, "Resolution Requirements in Stochastic Field Simulation of Turbulent Premixed Flames," Flow, Turbul. Combust., **101**(4), pp. 1103–1118.
[13] Schulz, O., Jaravel, T., Poinsot, T., Cuenot, B., and Noiray, N., 2017, "A Criterion to Distinguish Autoignition and Propagation Applied to a Lifted Methane–Air Jet Flame," Proc. Combust. Inst., **36**(2), pp. 1637–1644.
[14] Burke, U., Somers, K. P., O'Toole, P., Zinner, C. M., Marquet, N., Bourque, G., Petersen, E. L., Metcalfe, W. K., Serinyel, Z., and Curran, H. J., 2015, "An

Ignition Delay and Kinetic Modeling Study of Methane, Dimethyl Ether, and Their Mixtures at High Pressures," Combust. Flame, **162**(2), pp. 315–330.
[15] Lu, T., and Law, C. K., 2005, "A Directed Relation Graph Method for Mechanism Reduction," Proc. Combust. Inst., **30**(1), pp. 1333–1341.
[16] Lu, T., and Law, C. K., 2008, "Strategies for Mechanism Reduction for Large Hydrocarbons: N-Heptane," Combust. Flame, **154**(1–2), pp. 153–163.
[17] Kazakov, A., Chaos, M., Zhao, Z., and Dryer, F. L., 2006, "Computational Singular Perturbation Analysis of Two-Stage Ignition of Large Hydrocarbons," J. Phys. Chem. A, **110**(21), pp. 7003–7009.
[18] Versailles, P., Durocher, A., Bourque, G., and Bergthorson, J. M., 2019, "Measurements of the Reactivity of Premixed, Stagnation, Methane-Air Flames at Gas Turbine Relevant Pressures," ASME J. Eng. Gas Turbines Power, **141**(1), p. 011027.
[19] Ji, W., Ren, Z., and Law, C. K., 2019, "Evolution of Sensitivity Directions During Autoignition," Proc. Combust. Inst., **37**(1), pp. 807–815.
[20] Gordon, R. L., Masri, A. R., Pope, S. B., and Goldin, G. M., 2007, "A Numerical Study of Auto-Ignition in Turbulent Lifted Flames Issuing Into a Vitiated Co-Flow," Combust. Theory Modell., **11**(3), pp. 351–376.
[21] Gkagkas, K., and Lindstedt, R., 2007, "Transported PDF Modelling With Detailed Chemistry of Pre-and Auto-Ignition in CH_4/Air Mixtures," Proc. Combust. Inst., **31**(1), pp. 1559–1566.
[22] Lam, S., and Goussis, D., 1989, "Understanding Complex Chemical Kinetics With Computational Singular Perturbation," Symp. (Int.) Combust., **22**(1), pp. 931–941.
[23] Lu, T., Ju, Y., and Law, C. K., 2001, "Complex CSP for Chemistry Reduction and Analysis," Combust. Flame, **126**(1–2), pp. 1445–1455.
[24] Rehm, M., Seifert, P., and Meyer, B., 2009, "Theoretical and Numerical Investigation on the EDC-Model for Turbulence–Chemistry Interaction at Gasification Conditions," Comput. Chem. Eng., **33**(2), pp. 402–407.
[25] Lu, T., Yoo, C., Chen, J., and Law, C. K., 2010, "Three-Dimensional Direct Numerical Simulation of a Turbulent Lifted Hydrogen Jet Flame in Heated Coflow: A Chemical Explosive Mode Analysis," J. Fluid Mech., **652**, pp. 45–64.
[26] Xu, C., Park, J.-W., Yoo, C. S., Chen, J. H., and Lu, T., 2019, "Identification of Premixed Flame Propagation Modes Using Chemical Explosive Mode Analysis," Proc. Combust. Inst., **37**(2), pp. 2407–2415.
[27] Schulz, O., Piccoli, E., Felden, A., Staffelbach, G., and Noiray, N., 2019, "Autoignition-Cascade in the Windward Mixing Layer of a Premixed Jet in Hot Vitiated Crossflow," Combust. Flame, **201**, pp. 215–233.
[28] Scarinci, T., Freeman, C., and Day, I., "Passive Control of Combustion Instability in a Low Emissions Aeroderivative Gas Turbine," ASME Paper No. GT2004-53767.
[29] Kim, W.-W., and Menon, S., 1997, "Application of the Localized Dynamic Subgrid-Scale Model to Turbulent Wall-Bounded Flows," AIAA Paper No. 97-0210.
[30] Niemeyer, K. E., Curtis, N. J., and Sung, C.-J., 2017, "PyJac: Analytical Jacobian Generator for Chemical Kinetics," Comput. Phys. Commun., **215**, pp. 188–203.
[31] Strakey, P. A., and Eggenspieler, G., 2010, "Development and Validation of a Thickened Flame Modeling Approach for Large Eddy Simulation of Premixed Combustion," ASME J. Eng. Gas Turbines Power, **132**(7), p. 071501.
[32] Légier, J., Poinsot, T., Varoquié, B., Lacas, F., and Veynante, D., 2002, "Large Eddy Simulation of a Non-Premixed Turbulent Burner Using a Dynamically Thickened Flame Model," IUTAM Symposium on Turbulent Mixing and Combustion, Kingston, ON, Canada, June 3–6, pp. 315–326.
[33] O'Rourke, P. J., and Bracco, F. V., 1979, "Two Scaling Transformations for the Numerical Computation of Multidimensional Unsteady Laminar Flames," J. Comput. Phys., **33**(2), pp. 185–203.
[34] Schmalhofer, C. A., Griebel, P., and Aigner, M., 2018, "Influence of Autoignition Kernel Development on the Flame Stabilisation of Hydrogen-Nitrogen Mixtures in Vitiated Air of High Temperature," ASME Paper No. GT2018-7548.
[35] Lu, T., and Law, C. K., 2006, "Systematic Approach to Obtain Analytic Solutions of Quasi Steady State Species in Reduced Mechanisms," J. Phys. Chem. A, **110**(49), pp. 13202–13208.